can significantly improve the performance of colour-conversion devices.

In addition to applications as efficient colour converters, nanocrystals have been considered promising building blocks for colour-selectable optical-gain media in lasing applications[4]. One complication associated with lasing applications of nanocrystals is the requirement for extremely fast pumping that competes with non-radiative Auger recombination, leading to very short (picosecond) optical gain lifetimes[15]. So far, optical amplification and lasing in nanocrystals has been achieved using optical excitation with short laser pulses. Our estimations show that the 'energy-transfer pumping' scheme studied here provides carrier inflow that can in principle compete with non-radiative losses induced by Auger recombination. The energy-transfer rate of $\sim 2\,ns^{-1}$ measured for the uncapped quantum-well sample for $n_{eh} = 1.8 \times 10^{13}\,cm^{-2}$ results in a QW–NC carrier flux of $\sim 3.6 \times 10^{22}\,cm^{-2}s^{-1}$. For the nanocrystals of 1.9 nm radius studied here, the Auger recombination time is $\sim 50$ ps, which corresponds to a non-radiative carrier loss of $4 \times 10^{22}\,cm^{-2}s^{-1}$ for a close-packed monolayer. The latter value is comparable to the carrier inflow rate provided by energy transfer from the quantum well, indicating the feasibility of lasing in the energy-transfer pumping regime.

Although in this report we have studied optically pumped devices, it should be possible to realize the energy-transfer pumping scheme in the regime of electrical injection by combining nanocrystals with an electrically driven InGaN quantum well. The design of the quantum-well emitter in the 'energy-transfer colour-converter' (Fig. 4b) can be similar to that used in conventional InGaN light-emitting diodes, in which the quantum well is sandwiched between n- and p-doped GaN barriers with attached metal contacts[16]. Our preliminary studies indicate that we can fabricate relatively high mobility, thin (2–3 nm), n-doped GaN layers that can be used as top quantum-well barriers (adjacent to nanocrystals) in electrically powered devices. The direct comparison of photoluminescence dynamics in nanocrystals assembled on glass slides and n-doped GaN layers (up to $2 \times 10^{19}\,cm^{-3}$ doping level) do not show any noticeable quenching of nanocrystal emission in the presence of a proximal, doped semiconductor. Furthermore, the doping of the barriers is not expected to induce additional carrier losses in the quantum well[17,18]. All of these considerations strongly indicate the feasibility of high-efficiency, electrically driven, hybrid nanocrystal/quantum-well devices. □

1. Alivisatos, A. P. Semiconductor clusters, nanocrystals, and quantum dots. *Science* **271**, 933–937 (1996).
2. Murray, C. B., Norris, D. J. & Bawendi, M. G. Synthesis and characterization of nearly monodisperse CdE (E = S, Se, Te) semiconductor nanocrystallites. *J. Am. Chem. Soc.* **115**, 8706–8715 (1993).
3. Bruchez, M., Moronne, M., Gin, P., Weiss, S. & Alivisatos, A. P. Semiconductor nanocrystals as fluorescent biological labels. *Science* **281**, 2013–2016 (1998).
4. Klimov, V. I. *et al.* Optical gain and stimulated emission in nanocrystal quantum dots. *Science* **290**, 314–317 (2000).
5. *Next-Generation Lighting Initiative* http://lighting.sandia.gov/Xlightinginit.htm#snlngli
6. Colvin, V., Schlamp, M. & Alivisatos, A. Light-emitting diodes made from cadmium selenide nanocrystals and a semiconducting polymer. *Nature* **370**, 354–357 (1994).
7. Schlamp, M. C., Peng, X. G. & Alivisatos, A. P. Improved efficiencies in light emitting diodes made with CdSe(CdS) core/shell type nanocrystals and a semiconducting polymer. *J. Appl. Phys.* **82**, 5837–5842 (1997).
8. Coe, S., Woo, W.-K., Bawendi, M. & Bulovic, V. Electroluminescence from single monolayers of nanocrystals in molecular organic devices. *Nature* **420**, 800–803 (2002).
9. Dabbousi, B. O. *et al.* (CdSe)ZnS core-shell quantum dots: synthesis and characterization of a size series of highly luminescent nanocrystallites. *J. Phys. Chem.* **101**, 9463–9475 (1997).
10. Koleske, D. D. *et al.* Improved brightness of 380 nm GaN light emitting diodes through intentional delay of the nucleation island coalescence. *Appl. Phys. Lett.* **81**, 1940–1942 (2002).
11. Basko, D., La Rocca, G. C., Bassani, F. & Agranovich, V. M. Förster energy transfer from a semiconductor quantum well to an organic material overlayer. *Eur. Phys. J. B* **8**, 353–362 (1999).
12. Klimov, V. I. & McBranch, D. W. Femtosecond 1P-to-1S electron relaxation in strongly confined semiconductor nanocrystals. *Phys. Rev. Lett.* **80**, 4028–4031 (1998).
13. Xu, S., Mikhailovsky, A. A., Hollingsworth, J. A. & Klimov, V. I. Hole intraband relaxation in strongly confined quantum dots: Revisiting the "phonon bottleneck" problem. *Phys. Rev. B* **65**, 045319 (2002).
14. Klimov, V. I. Optical nonlinearities and ultrafast carrier dynamics in semiconductor nanocrystals. *J. Phys. Chem. B* **104**, 6112–6123 (2000).
15. Klimov, V. I., Mikhailovsky, A. A., McBranch, D. W., Leatherdale, C. A. & Bawendi, B. G. Quantization of multiparticle Auger rates in semiconductor quantum dots. *Science* **287**, 1011–1013 (2000).
16. Nakamura, S. & Fasol, G. *The Blue Laser Diode: GaN Based Light Emitters and Lasers* (Springer, Berlin Heidelberg, Germany, 1997).
17. Wu, L. W. *et al.* Influence of Si-doping on the characteristics of InGaN-GaN multiple quantum-well blue light emitting diodes. *IEEE J. Quantum Electron.* **38**, 446–450 (2002).
18. Bidnyk, S. *et al.* High-temperature stimulated emission in optically pumped InGaN/GaN multiquantum wells. *Appl. Phys. Lett.* **72**, 1623–1625 (1998).

..................................................................

# High levels of atmospheric carbon dioxide necessary for the termination of global glaciation

Raymond T. Pierrehumbert

*Department of the Geophysical Sciences, The University of Chicago, 5734 South Ellis Avenue, Chicago, Illinois 60637, USA*

.................................................................................................................................

**The possibility that the Earth suffered episodes of global glaciation as recently as the Neoproterozoic period, between about 900 and 543 million years ago, has been widely discussed[1–3]. Termination of such 'hard snowball Earth' climate states has been proposed to proceed from accumulation of carbon dioxide in the atmosphere[4]. Many salient aspects of the snowball scenario depend critically on the threshold of atmospheric carbon dioxide concentrations needed to trigger deglaciation[2,5]. Here I present simulations with a general circulation model, using elevated carbon dioxide levels to estimate this deglaciation threshold. The model simulates several phenomena that are expected to be significant in a 'snowball Earth' scenario, but which have not been considered in previous studies with less sophisticated models, such as a reduction of vertical temperature gradients in winter, a reduction in summer tropopause height, the effect of snow cover and a reduction in cloud greenhouse effects. In my simulations, the system remains far short of deglaciation even at atmospheric carbon dioxide concentrations of 550 times the present levels (0.2 bar of $CO_2$). I find that at much higher carbon dioxide levels, deglaciation is unlikely unless unknown feedback cycles that are not captured in the model come into effect.**

Whereas the problem of initiation of a 'hard snowball' climate state has received detailed attention[6–8], most current thinking about deglaciation is based on highly idealized energy balance model (EBM) calculations[9], which offer an accurate treatment of clear-sky radiation but neglect the seasonal cycle and fix cloud radiative forcing at its present value. Although 0.12 bar of $CO_2$ is often quoted as a representative deglaciation threshold, a closer reading of the work yields a threshold of 0.29 bar based on Neoproterozoic insolation (Fig. 2 of ref. 9). The same model but with slightly different choices of parameters[10] achieves deglaciation at only 0.16 bar. Because of the weak logarithmic dependence of radiative forcing on $CO_2$, the EBM results consistently imply that the system should be at least close to deglaciation at 0.2 bar of $CO_2$.

Four climatic characteristics crucially affect deglaciation, but are exceedingly difficult to estimate in simplified models. They are temperature lapse rate, cloud effects, dynamical heat transport and snow cover. Lapse rate, governed by a complex interplay of dynamics and convection, is crucial to the greenhouse effect, which can operate only insofar as the air aloft is significantly colder than the ground. Clouds are important because a high cloud over ice or snow reflects little more sunlight than the underlying surface, but provides a powerful warming effect through trapping of infrared radiation. EBM studies confirm the sensitivity of the deglaciation threshold to cloud assumptions[11]. Horizontal heat transport by atmospheric motion determines the extent to which the warm areas, which are the first to deglaciate, must give up some of their energy to the colder parts of the planet. Snow cover, determined by long-range transport of moisture in the atmosphere, affects the surface albedo, because snow is more reflective than sea ice[12].

The following results are based on general circulation model (GCM) simulations as described in the Methods section. The climate of the hard-snowball Earth is governed by the low thermal inertia of the globally solid surface, which has the consequence that the temperature responds primarily to the instantaneous solar radiation. The summer hemisphere becomes nearly isothermal, whereas the weakly illuminated winter hemisphere becomes extraordinarily cold, resulting in an extreme seasonal cycle resembling that of Mars[13,14]. Consider the January zonal mean near-surface air temperature for 100 p.p.m. $CO_2$ (Fig. 1). The south (summer) polar temperature is 228 K, only about 17 K cooler than the tropics, while the north (winter) polar temperature falls to 163 K. In July, the pattern is much the same, except reflected about the Equator, yielding a 64 K high-latitude seasonal cycle. During the equinoxes (not shown) the temperature is nearly symmetric about the Equator, with equatorial temperatures somewhat cooler than the summer subtropics, and polar temperatures somewhat warmer than those seen in Fig. 1 at the winter pole. Here I present results only for the solstice conditions, as a nearly identical discussion applies to the equinox.

$CO_2$ increase yields little warming in the winter hemisphere, and the summer temperature remains well short of the freezing point even at 0.2 bar of $CO_2$ (Fig. 1). Why is the warming so weak? Fig. 2 shows the diagnosed clear-sky greenhouse effect, defined as $G = \sigma T_s^4 - OLR_{clear}$, where $T_s$ is the surface temperature and $OLR_{clear}$ is the clear-sky outgoing longwave radiation. It is actually negative in

the winter extratropics, and grows only to modest values in the winter tropics. The reason for this behaviour is to be found in the vertical profile of temperature (Fig. 3). In the winter hemisphere, the atmosphere is nearly isothermal, because, in the absence of convection due to solar heating or a warm ocean, the atmosphere relaxes to radiative equilibrium, with a temperature inversion at the surface. Without colder air aloft, the winter hemisphere acts somewhat like the present-day stratosphere, which experiences a radiative cooling tendency in response to an increase of the $CO_2$ concentration. In the summer hemisphere, the low tropopause limits the vertical temperature contrast, yielding a weak greenhouse effect compounded by the virtual lack of water vapour feedback at such cold temperatures. As a result, at 0.2 bar of $CO_2$ the greenhouse trapping never attains even the $100\,W\,m^{-2}$ typical of the present low-$CO_2$ climate.

The cloud greenhouse effect (Fig. 2) is also weak, for two robust reasons: (1) the cloud greenhouse effect arises from high clouds, but even at saturation there is little water in the cold upper summer atmosphere, or at any level in the winter hemisphere; (2) the weak summer meridional temperature gradient cannot support the baroclinic eddies that lead to mid-latitude storm-track clouds in the modern climate. Significant cloud cover is limited primarily to the upward branch of the Hadley circulation, around 20° in the summer hemisphere. The cloud greenhouse effect barely exceeds $10\,W\,m^{-2}$, as compared to approximately $90\,W\,m^{-2}$ in the modern climate.

Dynamical heat transport due to the Hadley cell, and to a storm track at 30° in the winter hemisphere, draws energy out of the summer hemisphere. In January, the effect is equivalent to $45\,W\,m^{-2}$ of radiative cooling at 25°S in the 0.2 bar case.

Snow cover is a potent impediment to deglaciation. The tropical ice from about 10°N to 10°S is an ablation zone in all cases, losing water by sublimation. This water is accumulated as snow on the rest of the planet. The net snow accumulation is only about 0.5 cm liquid water equivalent per year, but over a mere decade the snow layer becomes deep enough to increase the albedo over most of the planet's surface. The interior of the tropical supercontinent remains devoid of snow, and warms the tropics through a reduction of the tropical surface albedo. The tropics are probably spuriously warm in this simulation. The bare tropical sea-ice is an artefact of the neglect of ice dynamics, as the extratropical snow and ice accumulation would eventually lead to sea-glacier flow, replacing the tropical sea ice with brighter glacial ice with an albedo of about 0.6 (refs 12, 15).
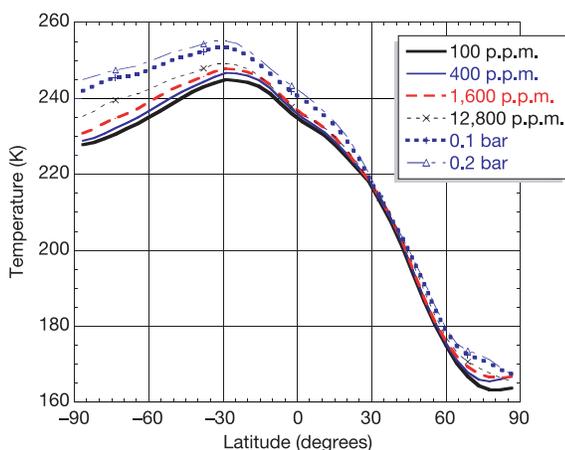


**Figure 1** January zonal-mean air temperature at the lowest model level, for various concentrations of atmospheric $CO_2$. Only sea-ice grid points are used in computing the mean, so as to focus on the temperature most relevant for determining deglaciation.
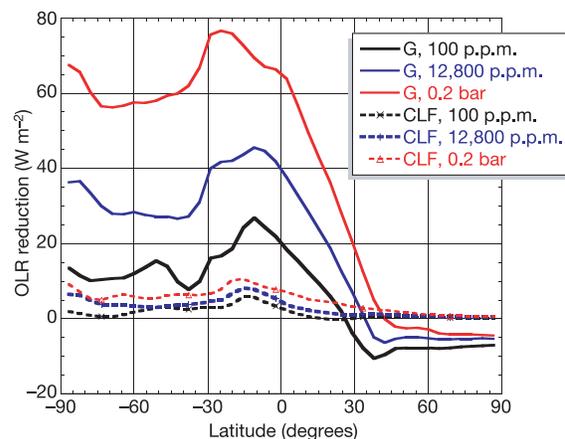


**Figure 2** January zonal-mean clear-sky greenhouse trapping (solid lines) and cloud longwave forcing (CLF) (dashed lines), for various $CO_2$ concentrations. The cloud longwave forcing is defined as the reduction in OLR caused by cloud effects, beyond the reduction caused by the clear-sky greenhouse effect.
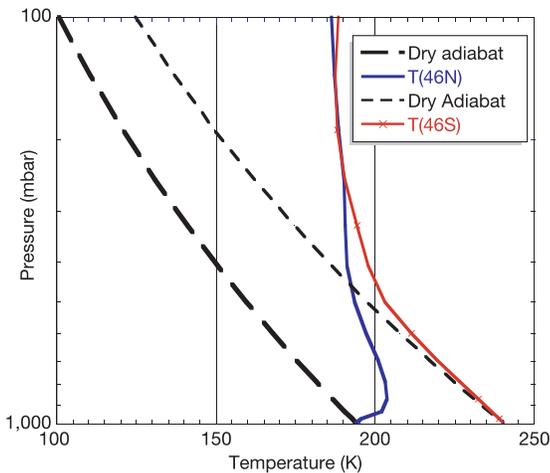
**Figure 3** Typical January vertical temperature profiles for the 100 p.p.m. $CO_2$ case. For reference, the dry adiabat (virtually identical to the moist adiabat at these temperatures) is shown. Convection resets the temperature to the adiabat, so by comparing the actual curves with the adiabat, we can identify the layer in which convection causes the familiar sharp drop of temperature with height. T(46N) and T(46S) represent respectively the temperature profiles at latitudes 46° N and 46° S.

Land glacier dynamics, neglected in this simulation, might cause the continent to become glaciated as well, leading to further cooling[16].

The aggregate of all the effects discussed above leaves the maximum air temperature 18 K short of the melting point at 0.2 bar; the ice surface temperature is nearly 10 K colder, owing to strong night-time cooling, and the equatorial deep ice temperature (which tracks the annual average) is colder still, resulting in the system being at least 30 K short of deglaciation. The present GCM cannot be reliably used above 0.2 bar, but if no new physical process enters to increase climate sensitivity, a logarithmic extrapolation suggests that each further doubling would warm the climate by about 2 K. At this rate, even 3.2 bar of $CO_2$ would be insufficient to trigger deglaciation. Assuming present outgassing rates[17] and assuming that two-thirds of outgassed $CO_2$ goes into the ocean[5], it would take 28 million years for 0.2 bar to accumulate in the atmosphere; accumulation of 1 or 2 bar would certainly not be impossible, but it would strain the limits of possibility.

It is far from certain that a hard-snowball state ever actually occurred on Earth, but the difficulty of deglaciation does not in itself rule out the possibility. There are several poorly understood physical feedbacks that may yet permit deglaciation. Alternative cloud parameterizations may retain more cloud water in the atmosphere. Also, above 0.2 bar, formation of $CO_2$ clouds becomes important and these can have a pronounced warming effect[18]. Greenhouse gases other than $CO_2$ may be important, or surface albedo may be reduced by admixture of dust, or by formation of leads in sea-glacier fracture zones or perhaps in thin-ice regions maintained by hydro-thermal plumes[19]. Even the suppressed convection that leads to weak vertical temperature contrast depends to some extent on surface flux parameterizations, the representation of the diurnal cycle and the convection scheme; future advances in the under-standing of cold-climate convection may yield different behavior. It is in this veiled area of physics that the prospect for recovery from a hard snowball lies hidden. □

## Methods

The simulations were carried out using the FOAM 1.5 GCM[8,20]. Once sea ice has built up to sufficient thickness, ocean dynamics has little effect. Hence, the simulations were carried out with a mixed-layer ocean without imposed horizontal oceanic heat transport. Run in this mode, FOAM is essentially a portable Beowulf-oriented re-implementation of

CCM3[21], run at R15 horizontal resolution (4.5° × 7.5°) with 18 levels. The solar luminosity was set at 94% of its present value, and the palaeogeography consists of an idealized equatorial supercontinent as in refs 8, 14. In the hard snowball, continental configuration affects climate almost exclusively through surface albedo, and even then only to the extent that land remains snow-free. The assumed configuration is highly favourable to deglaciation, as it puts dark bare land in the tropics where it can optimally receive insolation and transfer energy to the rest of the tropics. Orbital parameters were left at the Earth's present values. Surface albedo is specified in two spectral bands, with a broadband average value of 0.75 for snow (somewhat less than the new-snow value in ref. 12) and 0.5 for bare sea ice[12].

The model was first run at 100 p.p.m. $CO_2$ until the ocean became globally covered by sea ice of thickness of at least 5 m. Then, a sequence of 20-year simulations was carried out, with $CO_2$ concentration set at 400 p.p.m., 1,600 p.p.m., 1,2800 p.p.m., 10% (0.1 bar) and 20% (0.2 bar). Given the low thermal inertia of the ice/land surface, 20 years was found to be adequate for the climate to come into equilibrium with each $CO_2$ concentration. Results are taken from the last 10 years of each run. The only quantities that fail to reach equilibrium are the ice thickness and snow depth, but in neither case does the disequilibrium affect the climate. Snow continues to accumulate at up to 0.5 cm per year of liquid water equivalent, but as surface albedo saturates at a snow depth of only 0.5 cm over ice, the surface albedo has ample time to equilibrate in regions of net accumulation. To ensure that the ice/snow model retains adequate vertical resolution to treat the diurnal and seasonal cycle, ice thickness is clamped at a maximum of 20 m, and snow thickness at a maximum of 1 m (liquid water equivalent). This value is reached quickly, and given the low thermal diffusivity of ice, is sufficient to almost completely insulate the atmosphere from the heat content of the ocean. If allowed to grow, ice thickness would continue to increase at a rate of 20–50 cm yr$^{-1}$, further reducing the already small leakage of heat through the ice; the leakage through 20 m of ice causes the climate to be very slightly warmer than it would be if ice were allowed to reach its full thickness.

Although 1,600 p.p.m. is well within the range for which the CCM3 radiation code in FOAM is validated, there is little published basis on which to estimate the errors for $CO_2$ levels as high as 0.1 bar. To address this issue, we used a radiation model valid at high $CO_2$ (ref. 22) to recompute the outgoing longwave radiation (OLR) corresponding to a representative sampling of the temperature and humidity profiles produced by the GCM. The accurate OLR was then compared with the OLR produced by the GCM's internal radiation code. A typical comparison is shown in Supplementary Information. At 0.2 bar, the GCM radiation code over-estimates the correct OLR by at most 3.8 W m$^{-2}$ in the warmest months, with a mid-latitude annual mean error of 1.9 W m$^{-2}$.

1. Hoffman, P. F., Kaufman, A. J., Halverson, G. P. & Schrag, D. P. A Neoproterozoic snowball earth. *Science* **281**, 1342–1346 (1998).
2. Hoffman, P. F. & Schrag, D. P. The snowball Earth hypothesis: testing the limits of global change. *Terra Nova* **14**, 129–155 (2002).
3. Kennedy, M. J., Christie-Blick, N. & Sohl, L. E. Are Proterozoic cap carbonates and isotopic excursions a record of gas hydrate destabilization following Earth's coldest intervals? *Geology* **29**( 5), 443–446 (2001).
4. Kirschvink, J. L. in *The Proterozoic Biosphere; a Multidisciplinary Study* (eds Schorf, J. W. & Klein, C.) 51–52 (Cambridge Univ. Press, Cambridge, UK, 1992).
5. Higgins, J. A. & Schrag, D. P. Aftermath of a snowball Earth. *Geochem. Geophys. Geosyst.* **4**( 3), doi:10.1029/2002GC000403 (2003).
6. Chandler, M. A. & Sohl, L. E. Climate forcings and the initiation of low-latitude ice sheets during the Neoproterozoic Varanger glacial interval. *J. Geophys. Res. D* **105**, 20737–20756 (2000).
7. Hyde, W. T., Crowley, T. J., Baum, S. K. & Peltier, W. R. Neoproterozoic "snowball Earth" simulations with a coupled climate/ice-sheet model. *Nature* **405**, 425–429 (2000).
8. Poulsen, C., Pierrehumbert, R. T. & Jacob, R. Impact of ocean dynamics on the simulation of the Neoproterozoic "Snowball Earth". *Geophys. Res. Lett.* **28**( 8), 1575–1578 (2001).
9. Caldeira, K. & Kasting, J. F. Susceptibility of the early Earth to irreversible glaciation caused by carbon dioxide clouds. *Nature* **359**, 226–228 (1992).
10. Tajika, E. Faint young Sun and the carbon cycle: implication for the Proterozoic global glaciations. *Earth Planet. Sci. Lett.* **214**, 443–453 (2003).
11. Pierrehumbert, R. T. The hydrologic cycle in deep-time climate problems. *Nature* **419**, 191–198 (2002).
12. Warren, S. G., Brandt, R. E., Grenfell, T. C. & McKay, C. P. Snowball Earth: ice thickness on the tropical ocean. *J. Geophys. Res. C* **107**, doi:101029/2001JC001123 (2002).
13. Walker, J. C. G. *Earth System Processes, Abstr* 110–111 (Geological Society, London, 2001).
14. Jenkins, G. S. GCM greenhouse and high-obliquity solutions for early Proterozoic glaciation and middle Proterozoic warmth. *J. Geophys. Res. D* **108**, doi:101029/2001JD001582 (2003).
15. Goodman, J. C. & Pierrehumbert, R. T. Glacial flow of floating marine ice in Snowball Earth. *J. Geophys. Res.* **108**, doi:101029/2002JC001471 (2003).
16. Donnadieu, Y., Fluteau, F., Ramstein, G., Ritz, C. & Besse, J. Is there a conflict between the Neoproterozoic glacial deposits and the snowball Earth interpretation: an improved understanding with numerical modeling. *Earth Planet. Sci. Lett.* **208**, 101–112 (2003).
17. Zhang, Y. X. & Zindler, A. Distribution and evolution of carbon and nitrogen in Earth. *Earth Planet. Sci. Lett.* **117**, 331–345 (1993).
18. Forget, F. & Pierrehumbert, R. T. Warming early Mars with carbon dioxide clouds that scatter infrared radiation. *Science* **278**, 1273–1276 (1997).
19. Goodman, J. C., Collins, G. C., Marshall, J. & Pierrehumbert, R. T. Hydrothermal plume dynamics on Europa: Implications for chase formation. *J. Geophys. Res. E* **109**, doi:101029/2003JE002073 (2004).
20. Jacob, R. *Low Frequency Variability in a Simulated Atmosphere Ocean System*. Thesis, Univ. Wisconsin-Madison (1997).
21. Kiehl, J. T. *et al.* The National Center for Atmospheric Research Community. Climate Model: CCM3. *J. Clim.* **11**, 1131–1149 (1998).

22. Kasting, J. F., Pollack, J. B. & Ackerman, T. P. Response of Earth's atmosphere to increases in solar flux and implications for loss of water from Venus. *Icarus* **57**, 335–355 (1984).

· · · · · · · · · · · · · · · · · · · · · · · · · · · · · · · · · · ·

# Mesozoic origin for West Indian insectivores

Alfred L. Roca[1]*, Gila Kahila Bar-Gal[2]*, Eduardo Eizirik[2,3], Kristofer M. Helgen[4], Roberto Maria[5], Mark S. Springer[6], Stephen J. O'Brien[2] & William J. Murphy[1]

[1]*Laboratory of Genomic Diversity, Basic Research Program, SAIC-Frederick and* [2]*Laboratory of Genomic Diversity, National Cancer Institute, Frederick, Maryland 21702, USA* [3]*Centro de Biologia Genômica e Molecular, PUCRS, Porto Alegre, Brazil* [4]*School of Earth and Environmental Sciences, University of Adelaide, Adelaide 5005, Australia* [5]*Parque Zoologico Nacional, ZOODOM, Santo Domingo, Dominican Republic* [6]*Department of Biology, University of California, Riverside, California 92521, USA*

* These authors contributed equally to this work

· · · · · · · · · · · · · · · · · · · · · · · · · · · · · · · · · · ·

**The highly endangered solenodons, endemic to Cuba (*Solenodon cubanus*) and Hispaniola (*S. paradoxus*), comprise the only two surviving species of West Indian insectivores[1,2]. Combined gene sequences (13.9 kilobases) from *S. paradoxus* established that solenodons diverged from other eulipotyphlan insectivores 76 million years ago in the Cretaceous period, which is consistent with vicariance, though also compatible with dispersal. A sequence of 1.6 kilobases of mitochondrial DNA from *S. cubanus* indicated a deep divergence of 25 million years versus the congeneric *S. paradoxus*, which is consistent with vicariant origins as tectonic forces separated Cuba and Hispaniola[3,4]. Efforts to prevent extinction of the two surviving solenodon species would conserve an entire lineage as old or older than many mammalian orders.**

Solenodons are small (1 kg) fossorial (burrowing) insectivores, and are among the few native non-flying mammals that survived human settlement of the islands of the West Indies[1,2]. They inhabit the forests of Cuba and Hispaniola to elevations of 2,000 m, and shelter in caves, crevices, logs and extensive tunnel networks at a depth of >20 cm (refs 5 and 6). The dearth of Late Cretaceous or early Tertiary fossils from the West Indies has constrained resolution among alternative hypotheses regarding the origin of solenodons and their affinity to other mammals[1,7].

Some have suggested a close relationship to soricids (shrews) but not to talpids (moles)[8,9], or to soricids but not erinaceids (hedgehogs and gymnures)[9–11], and/or to fossil North American 'apternodontids' such as *Apternodus*, or geolabidids such as *Centetodon*[10,12–15]. A few authorities have suggested an affinity of solenodons to Afro-Malagasy tenrecs (both have zalambdodont molars)[12,15,16] and a trans-Atlantic dispersal event was suggested to explain this apparent relationship[12,16]. Recent molecular studies have placed the tenrecs firmly within Afrotheria, a superordinal mammalian group with

African origins[17,18], while placing shrews, moles and erinaceids in a distinct clade (Eulipotyphla) within Laurasiatheria, a superordinal mammalian group most probably of Northern Hemisphere origins[18]. For solenodons, only a few mtDNA sequences of *S. paradoxus* have been available for analyses; these have rejected a close affinity between solenodons and tenrecs[17]. One study has placed *Solenodon* as a sister group to soricids + talpids but not to erinaceids, although the bootstrap support for this placement (51%) was quite weak[17]; a second molecular analysis has positioned *Solenodon* as sister to a clade of rodents[19].

To examine the origin of *Solenodon* and its relationship to other mammals, we sequenced portions of 16 nuclear and three mitochondrial genes as previously described[18] using DNA extracted from a blood sample of a wild-born male *S. paradoxus* from the northern Dominican Republic (Cordillera Septentrional, Provincia de Espaillat), kept at the National Zoological Park (ZOODOM) in Santo Domingo. *S. paradoxus* DNA sequences were aligned (13,885 base pairs (bp) after removal of regions of ambiguous homology) to those of taxa from all extant eutherian orders of mammals[18]. Figure 1 depicts the phylogenetic position of solenodons relative to other eulipotyphlan insectivores (including the results of a separate analysis to place *S. cubanus*, see below). *Solenodon* grouped with eulipotyphlan insectivores with 100% maximum-likelihood bootstrap support and bayesian posterior probability (BPP) of 1.00. Putative affinities of *Solenodon* to tenrecs[12,15,16] or to rodents[19] received no support (Supplementary Information). There was high support for *Solenodon* being the most basal eulipotyphlan (95% maximum-likelihood bootstrap support; BPP of 1.00). *Solenodon* had a more basal position than had been suggested by previous molecular or morphological reports, relative to talpids[8,9] and/or to erinaceids[9–11,17].

We used well-established fossil dates[20] as minimum and maximum calibration points to estimate, using the method of Thorne–Kishino[21,22], the divergence date for *Solenodon* versus other placental mammals to be 76 million years (Myr) ago (95% credibility interval (CI) of 72–81 Myr ago) (Fig. 1 and Supplementary Information). The estimate for solenodon divergence (76 Myr ago) is comparable to or older than the estimated dates of some interordinal splits in mammals (for example, pangolins versus carnivores, or manatees versus elephants)[20], and considerably older than the basal divergence of most mammalian orders. The point estimate is 11 million years before the Cretaceous/Tertiary boundary at 65 Myr ago[3,7], with the 95% CI for solenodon divergence falling completely within the Mesozoic. The Mesozoic divergence date contrasts with previously reported support for Cenozoic divergence versus extant mainland forms for eight of nine distinct West Indian amphibian lineages, 67 of 68 reptile lineages, all 300–500 independent colonizations by birds, all 42 bat lineages, and the eight non-flying non-insectivore mammalian lineages[4].

West Indian insectivores are therefore the only tetrapod lineage for which strong evidence supports Mesozoic divergence versus extant mainland forms, with the possible exceptions of the frog genus *Eleutherodactylus* and the Cuban xantusiid lizard *Cricosaura typica*[4,7]. For the frog *Eleutherodactylus*, an intra-Antillean split within the genus has been previously dated to 70 ± 6.8 Myr ago[4]. For *Cricosaura typica* and related mainland lizards, we applied the Thorne–Kishino dating method[21,22] to previously published sequences[23]. While uncertain fossil constraints for xantusiids did not allow the definitive establishment of a Mesozoic origin for *Cricosaura* (95% CI of 57–101 Myr ago), the point estimate for the divergence of Cuban versus mainland xantusiids was 76 Myr ago (Supplementary Information).

Various biogeographic hypotheses have been proposed to account for the presence of solenodons only in the Antilles[12]. These invoke vicariance (biogeographic separation caused by the tectonic motion of land masses or rising sea levels) or dispersal (for example, rafting across the sea on vegetation) or some combination